Inorganic Chemistry

Article

pubs.acs.org/IC

Alkaline-Earth Metal Carboxylates Characterized by ^{43}Ca and ^{87}Sr Solid-State NMR: Impact of Metal-Amine Bonding

Kevin M. N. Burgess, Yang Xu, Matthew C. Leclerc, and David L. Bryce*

Department of Chemistry and Centre for Catalysis Research and Innovation, University of Ottawa, 10 Marie Curie Private, Ottawa, Ontario, Canada K1N 6N5

Supporting Information

ABSTRACT: A series of calcium and strontium complexes featuring aryl carboxylate ligands has been prepared and characterized by alkaline-earth (^{43}Ca and ^{87}Sr) solid-state NMR experiments in a magnetic field of 21.1 T. In the 11 compounds studied as part of this work, a range of coordination motifs are observed including nitrogen atom binding to Ca^{2+} and Sr^{2+}, a binding mode which has not been investigated previously by ^{43}Ca or ^{87}Sr solid-state NMR. ^{43}Ca isotopic enrichment has enabled the full characterization of the ^{43}Ca electric field gradient (EFG) and chemical shift tensors of the two calcium sites in calcium *p*-aminosalicylate (Ca(pams)), where both NMR interactions are affected by the presence of a nitrogen atom in the first coordination sphere of one of the metal sites. The ^{43}Ca isotropic chemical shift is sensitive to the Ca−N distance as exemplified by the NMR parameters of a second form of Ca(pams) and density functional theory (DFT) calculations. Studies of the strontium analogue, Sr(pams), confirm a similar sensitivity of the ^{87}Sr EFG tensor to the presence or absence of nitrogen in the first coordination sphere. To our knowledge, this is the first systematic ^{87}Sr NMR study of strontium complexes featuring organic ligands. The $|C_Q(^{87}Sr)|$ values are found to be sensitive to the coordination number about Sr^{2+}. In general, this work has also established a larger data set of reliable experimental $|C_Q(^{43}Ca)|$ values which correlate well with those obtained using gauge-including projector-augmented-wave (GIPAW) DFT calculations. It is found that the use of a recently recommended quadrupole moment for ^{43}Ca, −44.4 mbarn, improves the agreement with experimental values. This contribution lays the groundwork for the interpretation of ^{43}Ca and ^{87}Sr NMR spectra of more challenging systems, particularly where nitrogen−alkaline earth metal bonding is occurring.

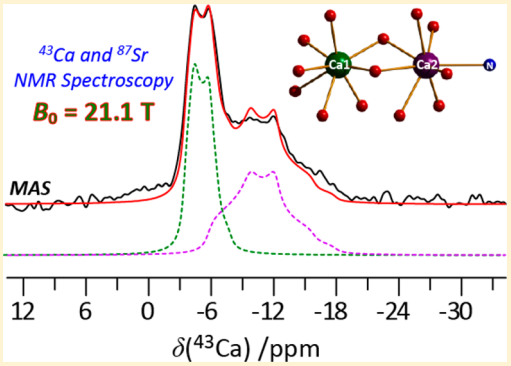

INTRODUCTION

The divalent calcium and strontium cations (Ca^{2+} and Sr^{2+}) have large abundances in Earth's crust and play important roles in many areas of chemistry, biochemistry, and materials science. For example, both cations are often present in the active sites associated with many biochemical processes including those in oxygen-evolving complexes such as photosystem II[1−3] and metalloproteins.[4,5] The alkaline-earth metal cations also play key roles in tunable fluorescent indicators,[6] ion sensing,[7] macrocyclic ion receptors,[8] and metal organic frameworks (MOFs) for selective CO_2 and N_2 adsorption.[9−11] Various groups have discussed the economic benefit of Ca^{2+} and Sr^{2+} over transition metals as catalysts for C−C or C−N bond formation,[12,13] often with chiral nitrogen-binding ligands.[14,15] The potential applications of calcium Grignard reagents[16] and allylcalcium complexes[17,18] are also currently under investigation.

Despite this plethora of applications, alkaline-earth metal solid-state nuclear magnetic resonance (SSNMR) is still a rather underdeveloped field specifically when attempting to relate certain NMR signatures to the structure or activity of a metal complex. In organic molecular environments, an increased dilution factor for Ca^{2+} and Sr^{2+} ions compared to some inorganic materials may hamper the acquisition of NMR spectra in a reasonable amount of time. Three recent reviews on alkaline-earth metal SSNMR[19−21] have aided in identifying the major pitfalls encountered when performing calcium and strontium NMR experiments. As summarized in Table 1,[22] both NMR active nuclei (^{43}Ca and ^{87}Sr) have very low Larmor frequencies ($\nu_L(^{43}Ca)$ = 26.93 MHz and $\nu_L(^{87}Sr)$ = 17.34 MHz

Table 1. Calcium and Strontium Nuclear Magnetic Resonance Properties[a]

property	^{43}Ca	^{87}Sr
spin quantum number, I	7/2	9/2
natural abundance/%	0.14	7.02
Larmor frequency at B_0 = 9.4 T/MHz	26.93	17.34
Larmor frequency at B_0 = 21.1 T/MHz	60.58	39.01
quadrupole moment, Q/mbarn[b]	−40.8 or −44.4[c]	305

[a]Nuclear magnetic resonance properties are from ref 22. [b]Quadrupole moments are summarized in ref 23. [c]An updated quadrupole moment for ^{43}Ca is reported in ref 67.

Received: October 22, 2013
Published: December 20, 2013

   dx.doi.org/10.1021/ic402658d | *Inorg. Chem.* 2014, 53, 552−561

when $\nu_L(^1H)$ = 400.13 MHz). The main challenge in ^{43}Ca NMR spectroscopy is its natural abundance of 0.14% (compared to 7.02% for ^{87}Sr), which is one of the smallest of all NMR-active nuclides in the periodic table. Powder NMR line shapes are also broadened in the solid state since both ^{43}Ca and ^{87}Sr are quadrupolar nuclei with spin quantum numbers, I, of 7/2 and 9/2, respectively. The nuclear electric quadrupole moment (Q), an intrinsic property of each nucleus, couples with the electric field gradient (EFG) resulting in a quadrupolar interaction (QI) that perturbs the Zeeman splitting and leads to broadening of the central transition (CT) resonance. The primary difficulty with ^{87}Sr NMR spectroscopy stems from its large quadrupole moment of 305 mbarn, whereas the currently accepted Q value for ^{43}Ca is much smaller (−40.8 mbarn).[23] The very low receptivity of each of these nuclides means that it is often impractical to record NMR spectra in a reasonable amount of time at standard magnetic field strengths.

Advancements in NMR technologies have resulted in the emergence of ultrahigh-field magnets (B_0 > 18.8 T) and thus an increase in the amenability of exotic low-γ nuclei such as ^{43}Ca and ^{87}Sr to NMR experiments. An array of studies are available in which Ca^{2+} ions present in biological materials have been probed by ^{43}Ca magic-angle spinning (MAS) NMR. These include materials containing alkyl/aryl boronate[24,25] and phosphonate ligands,[26] kidney stones[27] and calcium oxalate salts,[28] and other various organic ligands.[29] One impressive study from Laurencin et al. on calcium benzoate trihydrate (referred to in this work as Ca(ben)) employed ^{43}Ca isotopic labeling and experiments probing heteronuclear correlations such as transfer of population double resonance (TRAPDOR) between ^{43}Ca and ^{13}C nuclei.[30] Successful studies on other biologically relevant systems such as phosphates[31] and hydroxyapatite[32,33] have paved the way for the study of more challenging samples like bones, teeth,[34] and cement.[35] The ^{87}Sr nucleus, however, has not been studied as extensively because of its larger quadrupole moment. The most recent study by Bonhomme et al.[36] employs wideband, uniform rate, and smooth truncation (WURST) pulses coupled with quadrupolar Carr-Purcell-Meiboom-Gill (QCPMG) acquisition and ^{87}Sr isotopic labeling at high magnetic field strengths to characterize Sr^{2+} environments in Sr-doped Ca-silicate based bioglasses. In addition, the authors examined a number of organic and inorganic crystalline strontium phases.

Studies to date involving ^{43}Ca and ^{87}Sr SSNMR have focused mainly on oxygen coordination environments.[20] For example, researchers have correlated the average Ca−O distance of the first coordination sphere to the ^{43}Ca isotropic chemical shift, δ_{iso}.[37,38] There is, however, a relative dearth of studies involving coordination of Ca^{2+} and Sr^{2+} to other atoms, namely, nitrogen. Amino acids have been shown previously to bind to Ca^{2+} via their nitrogen atoms,[39−41] and so it is important to study such environments if we are to understand how ^{43}Ca and ^{87}Sr NMR spectroscopy can be useful in characterizing metalloproteins, which are constituted mainly of nitrogen-containing amino acids. In this work, we have prepared a series of Ca^{2+} and Sr^{2+} complexes containing various aryl and carboxylate ligands, illustrated in Scheme 1. The *p*-aminosalicylate (pams) and ethylenediaminetetraacetate (EDTA) ligands bind to the metal centers via their nitrogen atoms. ^{43}Ca and ^{87}Sr SSNMR experiments under stationary and/or MAS conditions are used in an attempt to correlate the presence of coordinated nitrogen atoms to changes in the alkaline-earth metal NMR parameters. We note that ^{25}Mg SSNMR has been used previously to examine Mg^{2+} centers featuring nitrogen coordination, for example, in porphyrins[42] and Mg_3N_2,[43] although these studies did not specifically investigate the role of nitrogen on the alkaline earth metal NMR parameters.

Scheme 1. Ligands Coordinated to Alkaline-Earth Metals in This Study[a]

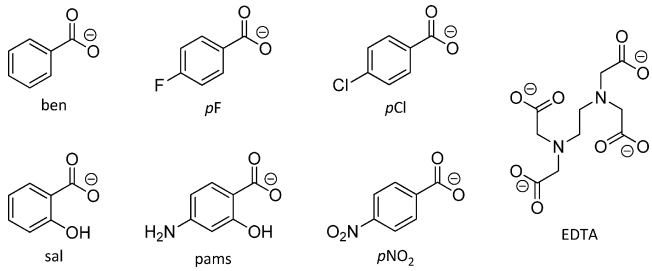

[a]The abbreviations are as follows: benzoate (ben), *p*-fluorobenzoate (*p*F), *p*-chlorobenzoate (*p*Cl), salicylate (sal), *p*-aminosalicylate (pams), *p*-nitrobenzoate (pNO_2), and ethylenediaminetetraacetate (EDTA).

We also corroborate our experimental findings with gauge-including projector-augmented-wave (GIPAW) density functional theory (DFT) calculations of the NMR parameters. This combined experimental-theoretical approach in NMR has found widespread usage especially in the field of alkaline-earth metal SSNMR because of the difficulties outlined above in interpreting NMR spectra of low-γ nuclei.[20] Because of the large data set of calcium compounds characterized by ^{43}Ca SSNMR in this study, in addition to currently available ^{43}Ca quadrupolar coupling constants (C_Q), we are able to establish a meaningful correlation between the calculated and experimental $C_Q(^{43}Ca)$ values.

EXPERIMENTAL DETAILS

Sample Preparation. Commercially available starting materials were used for the syntheses presented in this work. *p*-Fluorobenzoic acid (*p*F, ≥ 98.0%), *p*-chlorobenzoic acid (*p*Cl, ≥ 99.0%), *p*-nitrobenzoic acid (pNO_2, ≥ 98.0%), sodium benzoate (Na(ben), ≥ 99.5%), sodium salicylate (Na(sal), ≥ 99.5%), sodium *p*-aminosalicylate (Na(pams), ≥ 97.0%), ethylenediaminetetraacetic acid (H_4EDTA, ≥ 98.5%), calcium carbonate ($CaCO_3$, ≥ 99.0%), strontium carbonate ($SrCO_3$, ≥ 98.0%), calcium chloride ($CaCl_2$), strontium chloride ($SrCl_2$, ≥ 96.0%), and calcium acetate ($Ca(OAc)_2 \cdot H_2O$, ≥ 99.0%) were all purchased from Sigma-Aldrich and used without further purification.

The abbreviations AE(ligand), where AE = Ca or Sr and the ligands are presented in Scheme 1, are used for conciseness. Several of the samples are hydrates and the actual molecular formulas for each alkaline-earth metal complex are provided in the Supporting Information, Table S1. Ca(*p*F), Ca(*p*Cl), Sr(*p*Cl), and Sr(pNO_2) were synthesized using a previously reported method by Arlin et al.[44] wherein a 1:1 stoichiometric amount of substituted benzoic acid (1 g) and metal carbonate were dissolved in 20 mL of distilled water. The solution was stirred overnight, and the residual solids were filtered over a pad of Celite. The collected mother liquor was slowly evaporated at room temperature over several days or weeks to yield the appropriate crystalline salt.

Natural isotopic abundance samples of Ca(sal), Ca(pams), Sr(ben), Sr(sal), and Sr(pams) were prepared[44] by dissolving the appropriate amount of sodium salt (1 g) and alkaline-earth metal chloride in a 1:1 stoichiometric ratio in a minimum amount of distilled water. The mixture was stirred for several minutes and filtered over cotton. The resulting solution was slowly evaporated at room temperature until the appearance of transparent crystals. Isotopically enriched ^{43}Ca(pams) was synthesized in a similar way as described above using $^{43}CaCl_2$ (50

dx.doi.org/10.1021/ic402658d | Inorg. Chem. 2014, 53, 552−561

Table 2. Experimental and Calculated ^{43}Ca NMR Parameters for Organic Calcium Complexes[a]

compound	site	$\lvert C_Q(^{43}Ca)\rvert$ /MHz	η_Q	δ_{iso}/ppm[c]	Ω/ppm	κ
Ca(ben)[b]		**1.10(0.05)**	**0.7(0.1)**	**−2.5(0.2)**	**15(1)**	**0.75(0.10)**
		1.12	*0.68*	*−7*	*38*	*0.59*
Ca(*p*F)		**1.2(0.1)**	**0.6(0.2)**	**−2.3(0.2)**		
		0.94	*0.75*	*−4.9*	*37*	*0.53*
Ca(*p*Cl)		**1.3(0.1)**	**0.75(0.10)**	**−3.5(0.5)**		
		0.95	*0.85*	*−6.3*	*39*	*0.61*
Ca(sal)		**1.55(0.10)**	**0.50(0.10)**	**−4.0(0.5)**		
		1.58	*0.13*	*−5.9*	*42*	*−0.21*
Ca(pams)	**1**	**1.63(0.03)**	**0.35(0.05)**	**−3.2(0.5)**	**30(5)**	**−1.0(0.1)**
	1	*1.61*	*0.48*	*−6.0*	*37*	*−0.65*
	2[d]	**2.60(0.05)**	**0.60(0.03)**	**−5.5(0.5)**	**65(5)**	**0.6(0.1)**
	2	*2.37*	*0.64*	*−6.8*	*70*	*0.52*
Ca(pams)(OAc)		**1.15(0.05)**	**0.7(0.1)**	**5.4(0.2)**		
		1.24	*0.39*	*5.8*	*27*	*0.36*
Ca_2(EDTA)·7H_2O	**1**[e]	P_Q = **0.8(0.2)**		**6.1(0.8)**		
	1	*0.97*	*0.31*	*3.4*	*34*	*−0.24*
	2[e]	P_Q = **0.7(0.3)**		**15.1(0.4)**		
	2	*0.99*	*0.75*	*15.7*	*18*	*−0.20*

[a]Errors are given in parentheses. Experimental ^{43}Ca NMR parameters are in boldface and GIPAW DFT calculated results are italicized. [b]Experimental ^{43}Ca NMR parameters are from ref 30. Calculations were performed as part of this work. [c]The calculated σ_{iso} values were converted to chemical shifts using the relationship found in ref 63 (i.e., $\delta_{iso} = -0.8032\sigma_{iso} + 901.6$ ppm). [d]For this site, it was possible to determine the Euler angles which dictate the relative orientation of the EFG and CS tensor principal axis systems (α, β, γ = 210(20), 20(10), 110(10)°). For site 1 and other compounds, these angles were set to (α, β, γ = 0, 0, 0°) as the simulated line shape was not sensitive the values used. [e]Because of the absence of discernible line shapes, P_Q and δ_{iso} parameters were calculated using the method described in ref 20. An error of 1 ppm was used for both sites at 21.1 T and errors of 2 and 3 ppm (widths at approximately 90% peak height) were used for sites 1 and 2 respectively at 9.4 T. Standard deviations as a result of these errors are in parentheses.

mg) and 2.05 equiv of Na(pams), which were dissolved in a minimum amount of H_2O. To synthesize $^{43}CaCl_2$, a ^{43}Ca-labeled polymer chelate (donated by an industrial collaborator) was stirred in a 1 M HCl solution. The nondissolved polymer was filtered away and, upon solvent evaporation, a yellow oil was obtained. Twenty-five mg of this oil along with 25 mg of natural abundance $CaCl_2$ was used in the synthesis. We estimate the enrichment level of ^{43}Ca to be 4% based on comparison with NMR experiments performed at natural abundance for Ca(pams).

The Ca(pams)(OAc) analogue was synthesized in a similar way as Ca(pams), with $Ca(OAc)_2·H_2O$ as a source of calcium and 2 equiv of Na(pams) (1 g).[45] Ca_2(EDTA)·7H_2O was synthesized according to a literature procedure.[46] The phase purity of all synthesized alkaline-earth metal carboxylates was verified by comparing experimental powder X-ray diffraction patterns to those simulated with the available crystal structures (see Supporting Information, Figures S1 and S2 for Ca and Sr compounds, respectively).

Solid-State NMR Experiments. Solid-state NMR experiments were performed on all calcium and strontium samples at the National Ultrahigh-Field NMR Facility for Solids in Ottawa using a 21.1 T magnet (Bruker AVANCE II, $\nu_L(^1H)$ = 900.13 MHz, $\nu_L(^{43}Ca)$ = 60.6 MHz, $\nu_L(^{87}Sr)$ = 39.0 MHz). All ^{43}Ca NMR experiments at natural abundance were performed with a Bruker 7 mm MAS low-frequency double-resonance (HX) probe using a single pulse MAS experiment. In the case of ^{43}Ca(pams), a Bruker 4 mm MAS low-frequency double-resonance (HX) probe was used for one-pulse experiments under both MAS and stationary conditions. Continuous wave ^{1}H decoupling was used in certain cases. Experiments for strontium samples were performed using a home-built 7 mm low-frequency double-resonance (HX) probe and the WURST−QCPMG[47] pulse sequence with ^{1}H decoupling. For Sr(pams), it was necessary to perform a Solomon echo experiment[48] to observe a broader Sr^{2+} resonance because of its smaller spin−spin relaxation time constant, T_2. In this case, multiple pieces were acquired with varying transmitter offset frequencies using the variable offset cumulative spectra (VOCS) method.[49] These experiments were acquired using a modified Bruker broadband single channel probe. Chemical shifts were referenced to 0.00 ppm with a 1.0 M aqueous solution of $CaCl_2$[20] or $SrCl_2$. The CT-selective $\pi/2$ pulse lengths were those of the standard scaled by a factor of $1/(I + 1/2) = 1/4$ for ^{43}Ca and 1/5 for ^{87}Sr. Selective $\pi/4$ pulses were used in certain cases for natural abundance ^{43}Ca NMR experiments because of the uncertainty in the longitudinal relaxation time constant, T_1. In the case of Ca_2(EDTA)·7H_2O, the pulse length was calibrated directly on the sample.

Additional experiments were performed either at 9.4 T (Bruker AVANCE III, $\nu_L(^1H)$ = 400.13 MHz, $\nu_L(^{43}Ca)$ = 26.9 MHz) with a Bruker 7 mm MAS low-frequency double-resonance (HX) probe or at 11.75 T (Bruker AVANCE, $\nu_L(^1H)$ = 500.13 MHz, $\nu_L(^{43}Ca)$ = 33.7 MHz) with a Bruker 4 mm MAS low-frequency double-resonance (HX) probe. In all cases, single-pulse experiments were used. The chemical shift referencing and pulse calibrations were carried out analogously to the procedure described above. Specific experimental details pertaining to each compound in this work may be found in the Supporting Information, Tables S2 and S3.

Spectral Processing and Simulations. All spectra were recorded and processed using the Bruker TopSpin software (ver. 3.0). Most ^{43}Ca NMR spectra were left-shifted a small number of data points to remove signal due to probe ringing. The first echoes in all ^{87}Sr WURST−QCPMG experiments were removed also due to probe ringing, and spectra were analyzed in magnitude mode in the frequency domain. All individual pieces in the Solomon echo spectra of Sr(pams) are presented in magnitude mode and coadded in the frequency domain to yield the full spectrum. ^{43}Ca and ^{87}Sr spectra were simulated using the WSolids1 program (ver. 1.20.15).[50] Graphics were prepared with the aid of DMFit (ver. 2011).[51]

Computational Details. GIPAW DFT calculations were performed using ver. 4.1 of the CASTEP-NMR code (Accelrys Inc., San Diego, CA)[52,53] as implemented in the Materials Studio (Accelrys Inc.) software package (ver. 3.2). The available single crystal X-ray structure crystallographic information files (.cif) for each compound were used as input structures. The structures of Ca(*p*Cl), Ca(pams), Sr(ben), Sr(*p*Cl), Sr(pNO_2), and Sr(pams) are all from ref 44; those of Ca(sal) and Sr(sal) were reported by Debuyst et al.;[54] the structures of Ca(*p*F)[55] and Ca(ben)[56] were previously reported. The structure of

dx.doi.org/10.1021/ic402658d | Inorg. Chem. 2014, 53, 552−561

$Ca_2(EDTA)\cdot 7H_2O$ can be found in ref 46; some water molecules present in the lattice (i.e., not bound to Ca^{2+}) were assumed to have full occupancy for the calculations as these are not expected to affect greatly the calculated ^{43}Ca NMR parameters. Our structure for Ca(pams)(OAc), which has similar unit cell parameters to a previously reported one,[45] was used for the calculations. The *Pnma* space group for Ca(pams)(OAc) has a mirror plane bisecting the aryl ring, which creates disorder in the positioning of the hydroxyl group on the pams ligand. The disorder was removed manually and a modified .cif file was used for the calculations. The structures for Ca(D-gluconate)·$5H_2O$ and $Ca(C_2O_4)\cdot 3H_2O$ are taken from references 57 and 58, respectively. The generalized gradient approximation (GGA)[59] exchange-correlation functional of Perdew, Burke, and Ernzerhof (PBE) was used in all cases. On-the-fly generated pseudopotentials were employed for all atoms. All hydrogen atom positions were optimized prior to performing the NMR calculations. Many structures required a "coarse" setting for kinetic energy cutoff values and *k*-point grid because of the large unit cell volumes. Specific considerations for each calculation may be found in the Supporting Information, Table S4.

For nonperiodic DFT calculations, an isolated molecular model for Ca(pams) was built where both Ca^{2+} sites are present and benzoate ligands were converted to formate ligands. The nitrogen atom bound to calcium was hydrogen capped to make an ammonia ligand. A depiction of this model is found in Figure 5. The Gaussian '09 software package[60] was used for the DFT computations on the Ca(pams) model using the B3LYP hybrid functional and the 6-31+G* basis set on all atoms. Hydrogen positions were optimized prior to NMR calculations. Multiple NMR calculations were performed where the Ca–N distance was varied between 2.50 Å and 2.90 Å in 0.05 Å increments. The EFGShield program[61] was used to extract NMR parameters from the Gaussian '09 and CASTEP-NMR output files.

RESULTS AND DISCUSSION

^{43}Ca SSNMR Spectroscopy of Calcium Aryl Carboxylates. In Table 2 are presented the experimental and GIPAW DFT calculated ^{43}Ca EFG tensor and isotropic chemical shift parameters for all of the calcium carboxylate compounds considered in this work. Because of the absence of a discernible line shape at the higher magnetic field, some spectra were acquired at two magnetic field strengths. As for Ca(*p*Cl) and Ca(*p*F), both structures pack similarly to Ca(ben), which has already recently been extensively studied by ^{43}Ca SSNMR.[30] It is therefore not surprising that these three compounds exhibit similar experimental and calculated EFG tensor parameters (see Figure 1 for the NMR spectra). Inspection of all data in Table 2 shows that both the $|C_Q(^{43}Ca)|$ values (ranging from ~0.7 MHz in site 2 of $Ca_2(EDTA)\cdot 7H_2O$ to 2.60 MHz in site 2 of Ca(pams)) and δ_{iso} values (a total range of 22 ppm) change considerably depending on the nature of the carboxylate ligand bound to Ca^{2+}. This observation is supported by GIPAW DFT calculations (vide infra). Some specific insights obtained when relating the ^{43}Ca NMR parameters of the calcium carboxylates to their respective crystal structures are outlined below.

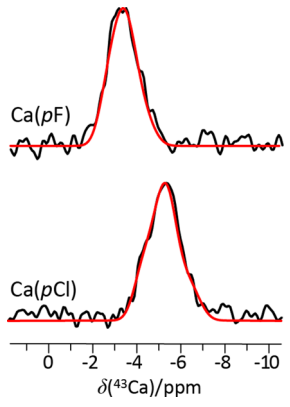

Figure 1. Natural abundance ^{43}Ca solid-state NMR spectra (in black) for Ca(*p*Cl) and Ca(*p*F) recorded at B_0 = 21.1 T under MAS conditions (ν_{rot} = 5 kHz). Analytical simulations (see Table 1) are in red. 9.4 T data are shown in the Supporting Information.

In Figure 2b is shown the natural abundance ^{43}Ca MAS NMR spectrum for Ca(sal) at 21.1 T. Also depicted in this figure is the immediate coordination environment of each Ca^{2+} ion from the reported single crystal X-ray structure.[54] The ^{43}Ca NMR spectrum for Ca(sal) is characterized by a single resonance, consistent with one crystallographic Ca site, with a $|C_Q(^{43}Ca)|$ value of 1.55 MHz. This resonance is very similar in shape to the more intense signal in the natural abundance ^{43}Ca NMR spectrum of Ca(pams) shown in Figure 2a. A qualitative comparison between the first coordination spheres about both Ca sites in Ca(pams) to that of Ca(sal) can be made: site 1 in Ca(pams) is very similar to Ca(sal) (i.e., both are 8-coordinate with oxygen atoms which form a distorted square face bicapped trigonal prism geometry about Ca^{2+}). It is also possible to observe a second broader resonance at natural abundance for Ca(pams) after quite a long experiment time of nearly 42 h (indicated by a dashed rectangle in Figure 2a). At this point, it was possible to assign this broader resonance to Ca site 2 in Ca(pams), which contains a nitrogen atom in its first coordination sphere. Since ^{43}Ca SSNMR has not been used previously to characterize Ca environments where nitrogen binding is present, we sought to isotopically label this sample (see Experimental Details) to accurately and precisely measure the EFG and CS tensor parameters for both Ca sites in Ca(pams) and relate these values to the calcium environments. Both MAS and stationary NMR spectra acquired at 21.1 T, along with a MAS spectrum at 11.75 T, are presented in Figure 3. From the MAS spectra, it is clear that two crystallographically unique sites are present in the structure in a 1:1 ratio with differing $|C_Q(^{43}Ca)|$ values of 1.63 and 2.60 MHz for sites 1 and 2, respectively. Both sites, however, have very similar experimental and calculated δ_{iso} values. It was also possible in

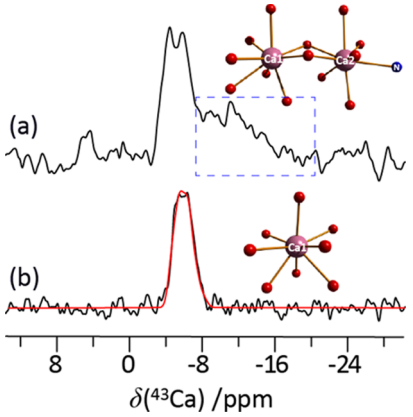

Figure 2. Natural abundance ^{43}Ca solid-state NMR spectra (in black) for Ca(sal) (b) and Ca(pams) (a) recorded at B_0 = 21.1 T under MAS conditions (ν_{rot} = 5 kHz). A dashed blue rectangle highlights a second broader ^{43}Ca resonance. In red is the analytical simulation for Ca(sal) in (b). The immediate coordination environment surrounding the Ca^{2+} sites in both compounds is also depicted. Calcium atoms are pink, oxygen atoms are red, and nitrogen atoms are blue.

dx.doi.org/10.1021/ic402658d | Inorg. Chem. 2014, 53, 552–561

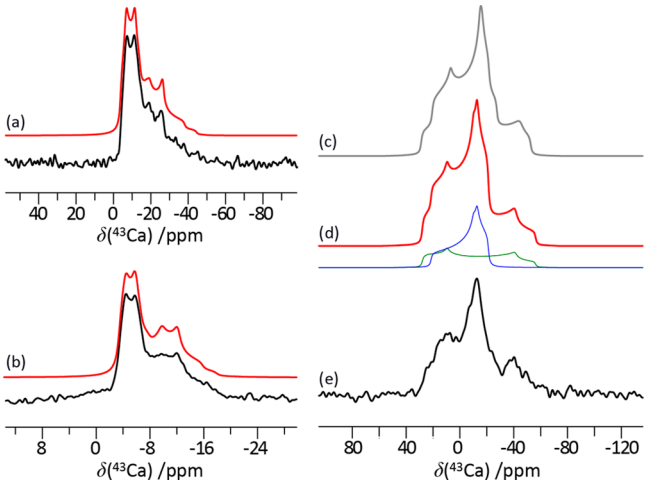

Figure 3. Experimental ^{43}Ca solid-state NMR experiments on isotopically enriched (~4%) ^{43}Ca(pams) acquired at B_0 = 21.1 T (b) and 11.75 T (a) under MAS conditions (ν_{rot} = 10 kHz) using single pulse experiments. Their respective analytical simulations are in red. In (e) is the ^{43}Ca NMR spectrum of the same sample acquired under stationary conditions with ^{1}H decoupling at B_0 = 21.1 T. The analytical simulation for the stationary NMR experiment is in (d), and a deconvolution is shown in blue and green for sites 1 and 2, respectively. The number of parameters required for the simulations in (d) was reduced as the quadrupolar parameters and δ_{iso} were constrained to values obtained from MAS experiments. In (c) is the line shape predicted from GIPAW DFT calculations.

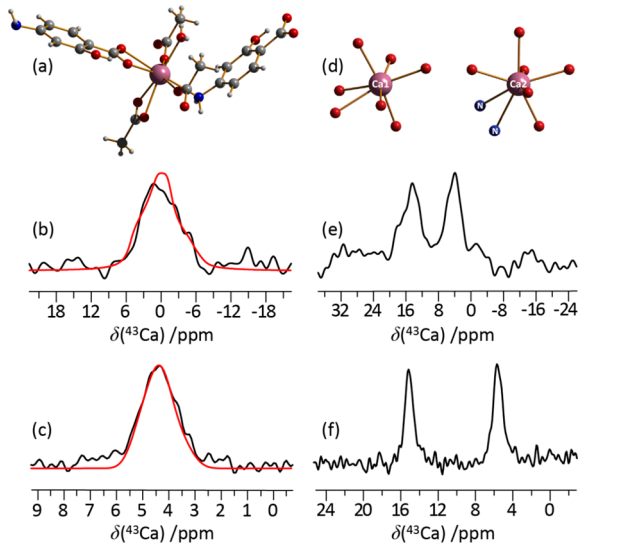

Figure 4. Natural abundance ^{43}Ca solid-state NMR spectra recorded at B_0 = 9.4 (b and e) and 21.1 T (c and f) under MAS conditions (ν_{rot} = 5 kHz) for Ca(pams)(OAc) [left] and Ca_2(EDTA)·7H_2O [right] respectively. Analytical simulations are in red. The structure of Ca(pams)(OAc) is depicted in (a), where a *p*-aminosalicylate ligand is bound to Ca via its nitrogen atom. The immediate coordination environment surrounding both Ca^{2+} sites in Ca_2(EDTA) is in (d). The two distinct Ca sites are clearly resolved for Ca_2(EDTA). Calcium atoms are pink, oxygen atoms are red, and nitrogen atoms are blue.

light of the GIPAW DFT calculations to characterize the CS tensor span, Ω, for both Ca sites in ^{43}Ca(pams). Very few ^{43}Ca SSNMR studies have reported chemical shift tensor parameters to date.[19−21] Widdifield et al.[62] have reported a Ω value of 31 ppm for anhydrous $CaCl_2$ whereas very characteristic chemical shift tensor parameters have been found for the three different anhydrous polymorphs of $CaCO_3$.[63] Site 2 in Ca(pams) (with N-coordination) exhibits one of the largest known Ω values of 65 ppm, whereas site 1 has a value of 30 ppm. Qualitatively, it is therefore clear that N-binding ligands can significantly alter both the ^{43}Ca EFG and the CS tensor parameters relative to the case where only oxygen atoms interact with the Ca^{2+} cation.

To further investigate how N-coordination may affect the ^{43}Ca NMR parameters more generally, we have synthesized a different Ca complex with the pams ligand and $Ca(OAc)_2$·H_2O as a source of Ca^{2+} ions. Ca(pams)(OAc) has one crystallographically unique Ca site which is 8-coordinate, including one N atom (see Figure 4a), like site 2 in Ca(pams). The OAc^- counteranions are also present in the lattice. Natural abundance ^{43}Ca MAS spectra acquired at 9.4 and 21.1 T confirm the presence of one Ca site (see Figures 4b and 4c respectively). Interestingly, a large decrease in the $|C_Q(^{43}Ca)|$ value (to 1.15 MHz) and an increase by approximately 10 ppm in the δ_{iso} value (5.4 ppm) are observed compared to site 2 in Ca(pams). Again, GIPAW DFT calculations (see Table 1) reproduce these experimental changes.

The EDTA ligand is known for its binding of various cations including alkaline-earth metals. In the case of Ca^{2+} chelation, the crystal structure of the Ca_2(EDTA)·7H_2O complex has two distinct Ca sites, where site 1 is fully coordinated by oxygen atoms and site 2 contains two nitrogen atoms in its first coordination sphere (see Figure 4d). The natural abundance ^{43}Ca MAS NMR spectrum was acquired at 21.1 T in a relatively short amount of experimental time (4 h) and has two featureless peaks that are clearly separated by approximately 10 ppm (see Figure 4f). Only the quadrupolar product, $|P_Q(^{43}Ca)|$ (i.e., $P_Q = C_Q(1 + (\eta_Q)^2/3)^{1/2}$), and the δ_{iso} values could be quantified even after acquiring a MAS spectrum at 9.4 T (see Figure 4e). The NMR parameters are reported in Table 2, and a significant difference in δ_{iso} values between both Ca sites (6.1 and 15.1 ppm for sites 1 and 2 respectively) is observed and reproduced with GIPAW DFT calculations. It was also possible to assign both resonances to the crystal structure on the basis of chemical shifts; site 2, which contains Ca−N bonds, corresponds to the more deshielded resonance.

It is not immediately clear how the ^{43}Ca δ_{iso} values are systematically affected by nitrogen coordination. In Ca(pams), the Ca^{2+} site with a nitrogen ligand is shielded by 2.3 ppm relative to the site which is fully coordinated by oxygen atoms, while in Ca_2(EDTA)·7H_2O, a deshielding of 9.0 ppm is observed for the site with two nitrogen ligands compared to the site which is fully coordinated by oxygen atoms. We were curious to see how changes in the Ca−N distance may affect the NMR parameters, as Ca(pams) (d_{Ca-N} = 2.7085 Å) and Ca(pams)(OAc) (d_{Ca-N} = 2.5813 Å) have δ_{iso} values of −5.5 and +5.4 ppm, respectively. Such a large difference in chemical shifts cannot be entirely accounted for by the change in the average Ca−O bond lengths for the two compounds (~0.03 Å) and the slope of −154 ppm/Å from model calculations on calcium organic compounds.[38] An isolated molecular model of Ca(pams) was built (see Figure 5a) and, after geometry optimization of the hydrogen atom positions, the Ca−N distance, d_{Ca-N}, was varied systematically from 2.50 to 2.90 Å (this is a representative range for Ca−N bond lengths in other similar complexes[39,64,65]) and the changes in the calculated NMR parameters were monitored. In Figure 5b is shown how the individual principal components of the ^{43}Ca CS tensor are affected by changing d_{Ca-N}. First, it is evident that a large

dx.doi.org/10.1021/ic402658d | *Inorg. Chem.* 2014, 53, 552−561

decrease in δ_{33} is observed compared to the changes in δ_{11} and δ_{22}. This in turn decreases the value of δ_{iso} as the Ca−N bond length is increased. This demonstrates the sensitivity of ^{43}Ca NMR toward small structural differences within the first coordination sphere of Ca^{2+} specifically when nitrogen atoms are involved in metal binding. While the ^{43}Ca chemical shift cannot be easily used to determine the number of nitrogen atoms in the first coordination sphere, it does appear to be diagnostic of the calcium−nitrogen distance. To compare the effect on the computed ^{43}Ca chemical shift of changing a single Ca−O distance vs a single Ca−N distance, the ammonia ligand in the model shown in Figure 5 was replaced by a water

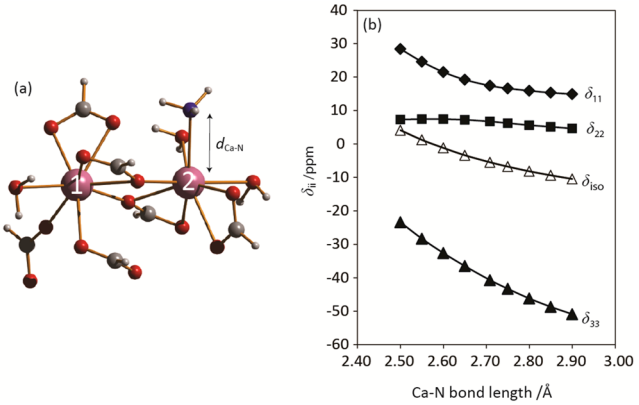

Figure 5. Calculated principal components of the ^{43}Ca chemical shift tensor as a function of the Ca−N distance (B3LYP/6-31+G*) (part (b)). A model system (part (a)) was built from the available crystal structure of Ca(pams) wherein both Ca sites are present and coordinated by water, formate, and ammonia ligands. All chemical shifts are relative to a calculation on the original structure of Ca(pams). An approximate range of 10 ppm for δ_{iso} is observed for a range of Ca−N distances between 2.50 and 2.90 Å. δ_{iso} changes by about −36 ppm/Å over this range. When visualizing the principal tensor components with respect to the molecular frame, δ_{33} is observed to be nearly perpendicular to the Ca−N bond vector, which explains the larger change in the value of δ_{33}.

molecule and the Ca−O distance was systematically varied over a range of typical values (2.30 to 2.70 Å). The ^{43}Ca chemical shift was found to be approximately equally sensitive to the varied distance for N-binding (−36 ppm/Å) and O-binding (−29 ppm/Å).

As summarized in a recent review by Moudrakovski,[21] reliable $|C_Q(^{43}Ca)|$ values are scarce, and many studies report only P_Q rather than C_Q values. Given the accurate characterization of the ^{43}Ca EFG tensor parameters in a larger data set of compounds as part of this work, a plot of the GIPAW DFT calculated $|C_Q(^{43}Ca)|$ values versus the experimentally determined values yields a useful correlation (Figure 6). This plot includes only reliable experimental $|C_Q(^{43}Ca)|$ values reported to date from the current and previous studies, which are summarized in the Supporting Information, Table S5.[28,29,3133,35,62,63,66] Furthermore, only data for compounds with high-quality structures from single-crystal X-ray or neutron diffraction are included. A rather good correlation is observed (R^2 = 0.910), but GIPAW DFT calculations seem to consistently underestimate the experimental values. Recently, a new value of Q for ^{43}Ca of −44.4 mbarn[67] has been proposed by combining the measured electric quadrupole hyperfine-structure constant and relativistic coupled-cluster calculations.

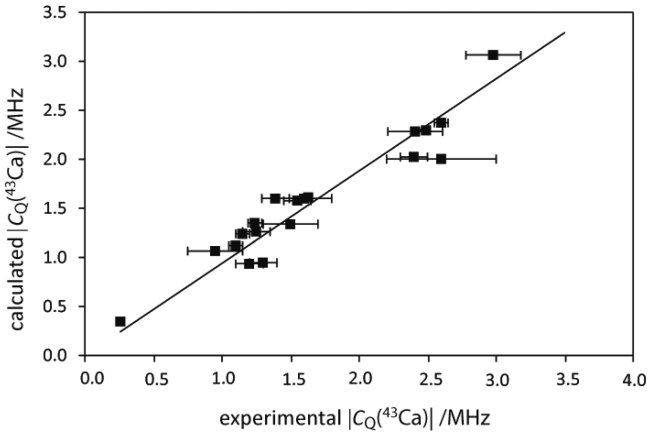

Figure 6. GIPAW DFT computed $|C_Q(^{43}Ca)|$ values versus the experimental values from this work and previously characterized Ca environments for which reliable ^{43}Ca SSNMR data are available (see main text for relevant references). Two plots were generated wherein the ^{43}Ca quadrupole moment is −40.8 mbarn ($|C_Q(^{43}Ca, calc.)| = 0.861|C_Q(^{43}Ca, exp.)|$, R^2 = 0.910) or −44.4 mbarn ($|C_Q(^{43}Ca, calc.)| = 0.937|C_Q(^{43}Ca, exp.)|$, R^2 = 0.910). Only the latter of the linear regressions is shown above for clarity. In both cases, the (0,0) data point was included in the linear regression.

One plot was generated using each Q value (only the graph where Q = −44.4 mbarn is shown in Figure 6). The slopes of the linear regressions are 0.861 and 0.937 for Q = −40.8 and −44.4 mbarn, respectively (recall, $C_Q = eV_{33}Q/h$). It is therefore recommended to use the updated quadrupole moment of −44.4 mbarn when performing calculations to improve the accuracy of the predicted ^{43}Ca EFG tensor parameters. This analysis will serve as a useful tool in future studies including those involving crystal structure refinements.

^{87}Sr WURST−QCPMG NMR of Strontium Aryl Carboxylates. Given the structural similarities between some calcium and strontium complexes, as well as the dearth of ^{87}Sr NMR information for strontium complexes bearing organic ligands, we next extended our work to the study of analogous strontium aryl carboxylate complexes. In total, ^{87}Sr SSNMR spectra were recorded for five strontium compounds. Spectra for Sr(ben), Sr(sal), Sr(pCl), and Sr(pNO$_2$), along with their respective analytical simulations, are shown in Figure 7. The experimental ^{87}Sr EFG tensor parameters and chemical shifts are reported in Table 3. We note that in all analytical simulations of ^{87}Sr NMR spectra, chemical shift anisotropy was not considered because of the dominance of the quadrupolar interaction. All spectra illustrated in Figure 7 were acquired using the WURST−QCPMG method at a magnetic field strength of 21.1 T. WURST pulses provided uniform and broadband excitation of the entire CT line shape in one transmitter offset setting (in our spectra, some line shapes spanned over 150 kHz at 21.1 T).[47] The very low receptivity of the ^{87}Sr nucleus prompted us to use the QCPMG method, which leads to the acquisition of multiple echoes in every scan and concentrates the signal intensity into spikelets to provide a spectrum with an increased signal-to-noise ratio when compared to the acquisition of a single echo. Because of increased quadrupolar broadening of the CT line shape and the low resonance frequency, experiments at lower magnetic field strengths (such as 9.4 T) were not feasible. The $|C_Q(^{87}Sr)|$ values, which range from 11.7 MHz for Sr(pNO$_2$) to 33.8 MHz for site 2 in Sr(pams), were found to be particularly sensitive to the local Sr^{2+} environment.

dx.doi.org/10.1021/ic402658d | Inorg. Chem. 2014, 53, 552−561

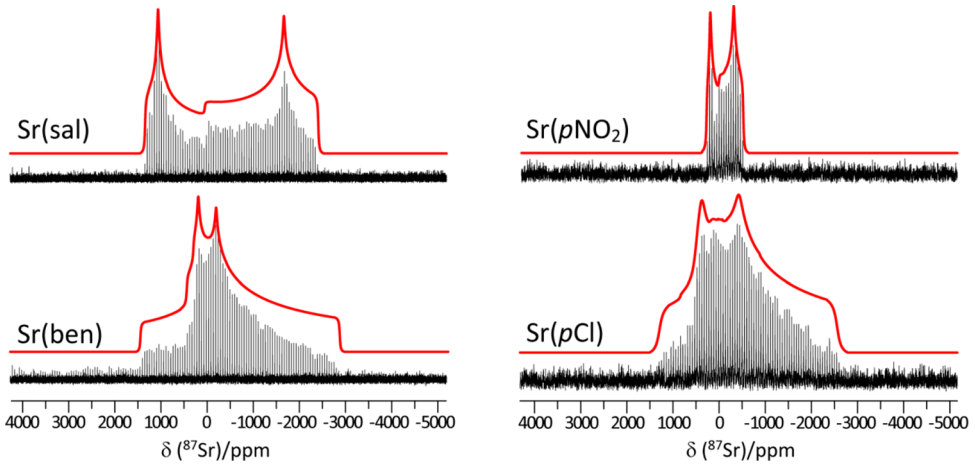

Figure 7. Experimental ^{87}Sr NMR spectra acquired at 21.1 T under stationary conditions using the WURST−QCPMG pulse sequence. Spikelet separations are 2 kHz for all samples. Partially excited satellite transitions are visible beyond the high-frequency discontinuity in the spectrum of Sr(ben). Red traces represent analytical simulations and NMR parameters are summarized in Table 3. Chemical shift anisotropy was not included in the simulations.

Table 3. Experimental and Calculated ^{87}Sr NMR Parameters for Strontium Aryl Carboxylates[a]

compound	space group	site	$\lvert C_Q(^{87}Sr)\rvert$ /MHz	η_Q	δ_{iso}/ppm[b]
Sr(ben)	$C2/c$		**22.5(0.5)**	**0.87(0.02)**	**0(50)**
		1	*20.7*	*0.76*	*−52*
		2	*20.8*	*0.84*	*−58*
Sr(pCl)	$P\bar{1}$		**22.2(0.2)**	**0.71(0.02)**	**0(50)**
			22.3	*0.69*	*−65*
Sr(sal)	$P2_1$		**26.1(0.3)**	**0.18(0.03)**	**30(20)**
			32.2	*0.45*	*−25*
Sr(pNO$_2$)	$P2_1/c$		**11.70(0.3)**	**0.25(0.05)**	**10(20)**
			15.3	*0.31*	*−30*
Sr(pams)	$P2_1/n$	**1**	**22.0(0.5)**	**0.92(0.02)**	**−50(30)**
		1	*22.0*	*0.86*	*−5*
		2	**33.8(0.3)**	**0.85(0.03)**	**150(50)**
		2	*35.1*	*0.65*	*−30*

[a]Errors are given in parentheses. Experimental ^{87}Sr NMR parameters are in boldface, and GIPAW DFT calculated results are italicized. [b]The calculated σ_{iso} values were converted to chemical shifts using the relationship found in ref 36 (i.e., $\delta_{iso} = -0.8750\sigma_{iso} + 2574$ ppm).

Isotropic chemical shifts could not be measured as precisely as in our ^{43}Ca experiments given the acquisition method and the ^{87}Sr spectral breadth. The experimental errors in the analytical simulations for δ_{iso} range from 20 to 50 ppm, which represents 10 to 25% of the total range (i.e., 200 ppm, see Table 3) of chemical shifts characterized as part of this work. Therefore, the establishment of meaningful correlations between δ_{iso} and the Sr^{2+} coordination environment is not feasible.

The WURST−QCPMG ^{87}Sr NMR spectrum of Sr(ben) shows one discernible Sr site characterized by a $\lvert C_Q(^{87}Sr)\rvert$ value of 22.5(0.5) MHz and an asymmetry parameter, η_Q, of 0.87. However, according to the X-ray crystal structure reported in the literature,[44] two distinct strontium sites are expected. GIPAW DFT calculations on this structure reveal very similar EFG tensor parameters for both sites, with $\lvert C_Q(^{87}Sr)\rvert$ values of 20.7 and 20.8 MHz and η_Q values of 0.76 and 0.84, for strontium sites 1 and 2, respectively. Structurally, both sites have nearly identical oxygen coordination environments but are mirror images of one another (see the Supporting Information, Figure S3). The ^{87}Sr NMR spectrum for Sr(ben) demonstrates one of the limitations of the WURST−QCPMG method in resolving sites which have very similar quadrupolar and chemical shift parameters. Sr(sal) ($P2_1$ space group) is characterized by a larger $\lvert C_Q(^{87}Sr)\rvert$ value of 26.1 MHz compared to Sr(pCl) ($P\bar{1}$ space group) and Sr(ben) ($C2/c$ space group) with $\lvert C_Q(^{87}Sr)\rvert$ values of 22.2 and 22.5 MHz, respectively. Qualitative inspection of the coordination geometry about Sr^{2+} in each of the three compounds does not reveal any obvious reason for the moderate variability in the ^{87}Sr quadrupolar coupling constants; indeed it has been shown recently that geometrical considerations about the immediate coordination sphere of Sr^{2+} alone do not fully account for changes in the value of $C_Q(^{87}Sr)$.[36] However, GIPAW DFT calculations prove to predict quite accurately these changes in the EFG tensor parameters (see Table 3).

The spectrum of Sr(pNO$_2$) is shown in Figure 7 and has the narrowest ^{87}Sr line shape considered in this work. It is characterized by a much smaller $\lvert C_Q(^{87}Sr)\rvert$ value of 11.7 MHz and hence fewer spikelets define the CT line shape. GIPAW DFT calculations also predict a lowering of the $\lvert C_Q(^{87}Sr)\rvert$ value for Sr(pNO$_2$) relative to the compounds discussed above, but the calculations overestimate the experimental datum by several MHz (Table 3). This overestimation might be due to the presence of a larger number of coordinated water molecules (i.e., 7 in this case) about the Sr^{2+} cation compared to the other compounds considered in this work. Dynamics of coordinated water molecules are not accounted for in our calculations (performed at 0 K) and have been shown to affect quadrupolar parameters in previous SSNMR studies involving Mg^{2+} coordinated to organic-functionalized carboxylate ligands.[68] More interestingly, Sr(pNO$_2$) is 9-fold coordinated with oxygen atoms whereas Sr(ben), Sr(sal), Sr(pCl), and site 1 of Sr(pams) are all coordinated to 8 oxygen atoms. A lower value of $\lvert C_Q(^{87}Sr)\rvert$ for Sr(pNO$_2$) is consistent with a few previously characterized 9-oxygen coordinated strontium sites such as those in $SrCO_3$ ($\lvert C_Q(^{87}Sr)\rvert$ = 8.91 MHz)[69] and a micaceous mineral ($\lvert C_Q(^{87}Sr)\rvert$ = 9.02 MHz).[70] However, the previously studied strontium malonate[36] is 9-coordinate[71] and has a larger $\lvert C_Q(^{87}Sr)\rvert$ value of 31.5 MHz. Both oxygen coordination polyhedra surrounding Sr(pNO$_2$) and strontium malonate are monocapped square antiprisms. The latter complex has,

dx.doi.org/10.1021/ic402658d | Inorg. Chem. 2014, 53, 552−561

qualitatively, a much larger degree of distortion, which explains the large difference between the $|C_Q(^{87}Sr)|$ values.

The final Sr compound in our series, Sr(pams), has a molecular and crystal structure that resembles closely its calcium analogue, Ca(pams) (see Supporting Information, Figure S4 for a comparison). Both structures crystallize in the $P2_1/n$ space group and have two crystallographically unique metal cation sites. As is the case for Ca(pams), site 1 in Sr(pams) is fully coordinated by oxygen atoms, and site 2 has seven oxygen atoms and 1 nitrogen atom in the first coordination sphere. Our first attempt at acquiring this ^{87}Sr spectrum was in the same manner as for the other Sr compounds in this study. The ^{87}Sr WURST−QCPMG spectrum is shown in Figure 8b and resembles quite closely

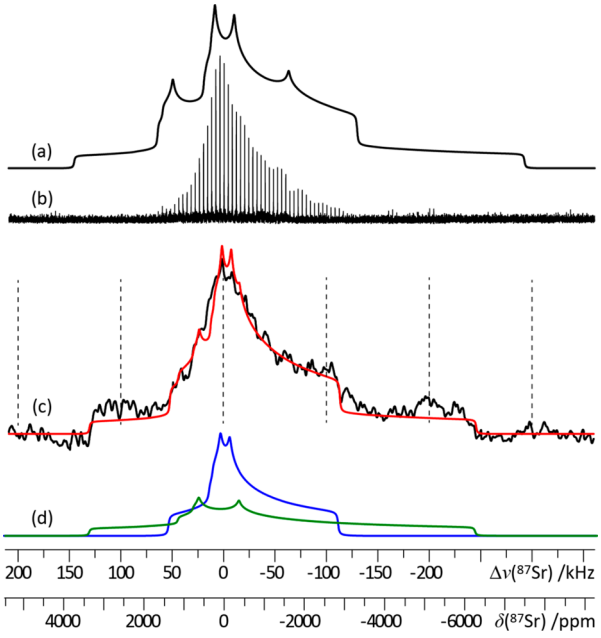

Figure 8. Experimental ^{87}Sr WURST−QCPMG NMR spectrum of Sr(pams) acquired at 21.1 T (b) and simulation of the GIPAW DFT calculated ^{87}Sr NMR spectrum under stationary conditions (a). Only the NMR parameters for the narrower Sr line shape can be estimated using this method. A stepped solid echo experiment was performed at 21.1 T (c, black trace) and a simulation with two strontium sites in a 1:1 ratio is shown in red. The deconvolution of the simulation from (c) is depicted in (d) where site 1 is in blue and site 2 is in green. Dashed lines indicate transmitter offset frequency settings for VOCS data acquisition.

the spectrum observed for Sr(ben) with an asymmetry parameter near unity and a $|C_Q(^{87}Sr)|$ value of ∼22 MHz. The observation of a single Sr site is in disagreement with the reported crystal structure, which has two crystallographically unique Sr^{2+} cations. Furthermore, unlike for Sr(ben), the GIPAW DFT calculations predict substantially different $|C_Q(^{87}Sr)|$ values for Sr(pams); these are 22.0 and 35.1 MHz for sites 1 and 2 respectively (see Figure 8a for a simulation based on the calculated NMR parameters). The larger $|C_Q(^{87}Sr)|$ value is in agreement with what is observed for Ca(pams) where site 2, which contains the alkaline-earth metal-bound nitrogen atom, is characterized by a C_Q value about 1.5 times larger than that for site 1. We were unable to observe the second broader site in the ^{87}Sr NMR spectrum even when stepping the transmitter offset frequency in the WURST−QCPMG experiment. The reason for this is likely a smaller T_2 value for site 2. Instead, a solid echo experiment was successfully used to acquire the spectrum of both strontium sites (see Figure 8c). For this spectrum, multiple transmitter offset settings were required to obtain the full CT line shape, with a spectral breadth of nearly 400 kHz. The singularities in this spectrum confirm the presence of a second Sr site with a larger $|C_Q(^{87}Sr)|$ value of 33.8 MHz. The observation of this broader site is in agreement with the GIPAW DFT calculations and thus the larger C_Q value can be attributed to the presence of a nitrogen atom coordinated to Sr^{2+} as was shown for the Ca(pams) analogue. As shown with this example, care must be taken when performing WURST−QCPMG experiments on Sr samples as T_2 values may affect our ability to observe Sr^{2+} in certain chemical environments.

CONCLUSIONS

In summary, we have presented a ^{43}Ca and ^{87}Sr solid-state NMR study on the Ca^{2+} and Sr^{2+} cations present in various organic molecular environments which may serve as models for metal organic frameworks, metal ion receptors, and biological systems. The benzoate, salicylate, and ethylenediaminetetraacetate (EDTA) ligands employed in this study allow for a variety of coordination motifs to be probed by alkaline-earth metal solid-state NMR spectroscopy including nitrogen binding to the metal centers. It was shown with the examples of Ca(pams), its derivative, Ca(pams)(OAc), and Sr(pams) that both the electric field gradient and chemical shift tensors are sensitive to the presence of alkaline earth metal−nitrogen interactions. For example, DFT computations on a model for Ca(pams) demonstrated an inverse correlation between the calcium chemical shift and the Ca−N bond length which is consistent with the trend observed experimentally for Ca(pams) and Ca(pams)(OAc). It was also possible to fully characterize the ^{43}Ca chemical shift tensors of both crystallographically unique sites in Ca(pams) with the aid of ^{43}Ca isotopic labeling. A structural assignment could be made with the aid of GIPAW DFT computations that predicted larger chemical shift anisotropy and $|C_Q(^{43}Ca)|$ values for the Ca^{2+} interacting with a nitrogen atom in its first coordination sphere.

Many previous studies have been unsuccessful in fully characterizing accurate ^{43}Ca EFG tensor parameter (i.e., by only reporting P_Q values for example), thus prohibiting until now the establishment of a meaningful correlation between DFT calculated and experimental $|C_Q(^{43}Ca)|$ values for future crystal structure refinement purposes. Our study has also allowed for the accurate characterization of both the ^{43}Ca quadrupolar coupling constants and asymmetry parameters. The best agreement was observed between the GIPAW DFT calculated $|C_Q(^{43}Ca)|$ values and experiment when using the newly proposed quadrupole moment for ^{43}Ca, $Q = -44.4$ mbarn, suggesting that this value be used in such studies going forward.

Finally, ^{87}Sr WURST−QCPMG NMR was used to characterize a series of analogous organic strontium complexes. It was found that, in general, for ^{87}Sr NMR, the EFG tensor is the most sensitive parameter to minute structural changes as was evidenced by both Sr(*p*Cl) and Sr(sal). This is consistent with the recent findings of Bonhomme et al.[36] In the case of Sr(*p*NO_2), the smaller $|C_Q(^{87}Sr)|$ value was attributed to a more symmetric 9-oxygen coordinate monocapped square antiprism geometry. As for Sr(pams), changes in the ^{87}Sr NMR acquisition method allowed us to observe the second broader

dx.doi.org/10.1021/ic402658d | *Inorg. Chem.* 2014, 53, 552−561

NMR line shape associated with the nitrogen-binding Sr site. Good agreement between experiment and GIPAW DFT calculations was also noted for ^{87}Sr NMR parameters. This contribution has allowed for a deeper understanding of how subtle structural changes about alkaline-earth metal cations are manifested in their NMR parameters, and may find use in future studies involving these essential elements which play key roles in metalloproteins and more affordable alkaline-earth metal catalysts, to name but a few applications.

■ ASSOCIATED CONTENT

Supporting Information

Powder X-ray diffractograms for all Ca and Sr compounds; immediate coordination polyhedra for Sr(ben), Ca(pams), and Sr(pams); compound abbreviations and full formulas; experimental ^{43}Ca and ^{87}Sr SSNMR conditions; spectra obtained at 9.4 T; computational details for GIPAW DFT calculations; summary of data for Figure 6. This material is available free of charge via the Internet at http://pubs.acs.org.

■ AUTHOR INFORMATION

Corresponding Author

*E-mail: dbryce@uottawa.ca. Phone: +1 613 562 5800, ext. 2018. Fax: +1 613 562 5170

Notes

The authors declare no competing financial interest.

■ ACKNOWLEDGMENTS

K.M.N.B. and Y.X. thank the Natural Sciences and Engineering Research Council (NSERC) of Canada for graduate and undergraduate scholarships, respectively. D.L.B. thanks NSERC, the Canada Foundation for Innovation, and the Ontario Ministry of Research and Innovation for funding. We thank Dr. Glenn A. Facey, Dr. Ilia Korobkov, Dr. Tara Kell, and Dr. Victor Terskikh for technical support, and Dr. Igor Moudrakovski for helpful comments. Access to the 900 MHz NMR spectrometer was provided by the National Ultrahigh-Field NMR Facility for Solids (Ottawa, Canada), a national research facility funded by the Canada Foundation for Innovation, the Ontario Innovation Trust, Recherche Québec, the National Research Council Canada, and Bruker BioSpin and managed by the University of Ottawa (www.nmr900.ca). NSERC is acknowledged for a Major Resources Support grant.

■ REFERENCES

(1) Gatt, P.; Petrie, S.; Stranger, R.; Pace, R. J. *Angew. Chem., Int. Ed.* **2012**, *51*, 12025−12028.
(2) Tsui, E. Y.; Tran, R.; Yano, J.; Agapie, T. *Nat. Chem.* **2013**, *5*, 293−299.
(3) Park, Y. J.; Cook, S. A.; Sickerman, N. S.; Sano, Y.; Ziller, J. W.; Borovik, A. S. *Chem. Sci.* **2013**, *4*, 717−726.
(4) Babu, C. S.; Dudev, T.; Lim, C. *J. Am. Chem. Soc.* **2013**, *135*, 6541−6548.
(5) Hoi, H.; Matsuda, T.; Nagai, T.; Campbell, R. E. *J. Am. Chem. Soc.* **2013**, *135*, 46−49.
(6) Collot, M.; Loukou, C.; Yakovlev, A. V.; Wilms, C. D.; Li, D.; Evrard, A.; Zamaleeva, A.; Bourdieu, L.; Léger, J.-F.; Ropert, N.; Eilers, J.; Oheim, M.; Feltz, A.; Mallet, J.-M. *J. Am. Chem. Soc.* **2012**, *134*, 14923−14931.
(7) Bar-Shir, A.; Gilad, A. A.; Chan, K. W. Y.; Liu, G.; van Zijl, P. C. M.; Bulte, J. W. M.; McMahon, M. T. *J. Am. Chem. Soc.* **2013**, *135*, 12164−12167.
(8) Sleem, H. F.; Dawe, L. N.; Georghiou, P. E. *New J. Chem.* **2012**, *36*, 2451−2455.
(9) Banerjee, D.; Zhang, Z.; Plonka, A. M.; Li, J.; Parise, J. B. *Cryst. Growth Des.* **2012**, *12*, 2162−2165.
(10) Zhang, X.; Huang, Y.-Y.; Zhang, M.-J.; Zhang, J.; Yao, Y.-G. *Cryst. Growth Des.* **2012**, *12*, 3231−3238.
(11) Yeh, C.-T.; Lin, W.-C.; Lo, S.-H.; Kao, C.-C.; Lin, C.-H.; Yang, C.-C. *CrystEngComm* **2012**, *14*, 1219−1222.
(12) Begouin, J.-M.; Niggemann, M. *Chem.—Eur. J.* **2013**, *19*, 8030−8041.
(13) Brinkmann, C.; Barrett, A. G. M.; Hill, M. S.; Procopiou, P. A. *J. Am. Chem. Soc.* **2012**, *134*, 2193−2207.
(14) Tsubogo, T.; Yamashita, Y.; Kobayashi, S. *Chem.—Eur. J.* **2012**, *18*, 13624−13628.
(15) Kobayashi, S.; Yamashita, Y. *Acc. Chem. Res.* **2011**, *44*, 58−71.
(16) Köler, M.; Langer, J.; Fischer, R.; Görls, H.; Westerhausen, M. *Chem.—Eur. J.* **2013**, *19*, 10497−10500.
(17) Jochmann, P.; Dols, T. S.; Spaniol, T. P.; Perrin, L.; Maron, L.; Okuda, J. *Angew. Chem., Int. Ed.* **2009**, *48*, 5715−5719.
(18) Jochmann, P.; Maslek, S.; Spaniol, T. P.; Okuda, J. *Organometallics* **2011**, *30*, 1991−1997.
(19) Bryce, D. L. *Dalton Trans.* **2010**, *39*, 8593−8602.
(20) Laurencin, D.; Smith, M. E. *Prog. Nucl. Magn. Reson. Spectrosc.* **2013**, *68*, 1−40.
(21) Moudrakovski, I. L. *Annu. Rep. NMR Spectrosc.* **2013**, *79*, 129−240.
(22) Harris, R. K.; Becker, E. D.; Cabral de Menezes, S. M.; Goodfellow, R.; Granger, P. *Pure Appl. Chem.* **2001**, *73*, 1795−1818.
(23) Pyykkö, P. *Mol. Phys.* **2008**, *106*, 1965−1974.
(24) Reinholdt, M.; Croissant, J.; Di Carlo, L.; Granier, D.; Gaveau, P.; Bégu, S.; Devoisselle, J.-M.; Mutin, P. H.; Smith, M. E.; Bonhomme, C.; Gervais, C.; van der Lee, A.; Laurencin, D. *Inorg. Chem.* **2011**, *50*, 7802−7810.
(25) Sene, S.; Reinholdt, M.; Renaudin, G.; Berthomieu, D.; Zicovich-Wilson, C. M.; Gervais, C.; Gaveau, P.; Bonhomme, C.; Filinchuk, Y.; Smith, M. E.; Nedelec, J.-M.; Bégu, S.; Mutin, P. H.; Laurencin, D. *Chem.—Eur. J.* **2013**, *19*, 880−891.
(26) Sene, S.; Bouchevreau, B.; Martineau, C.; Gervais, C.; Bonhomme, C.; Gaveau, P.; Mauri, F.; Bégu, S.; Mutin, P. H.; Smith, M. E.; Laurencin, D. *CrystEngComm* **2013**, *15*, 8763−8775.
(27) Bowers, G. M.; Kirkpatrick, R. J. *Cryst. Growth Des.* **2011**, *11*, 5188−5191.
(28) Colas, H.; Bonhomme-Coury, L.; Diogo, C. C.; Tielens, F.; Babonneau, F.; Gervais, C.; Bazin, D.; Laurencin, D.; Smith, M. E.; Hanna, J. V.; Daudon, M.; Bonhomme, C. *CrystEngComm* **2013**, *15*, 8840−8847.
(29) Wong, A.; Howes, A. P.; Dupree, R.; Smith, M. E. *Chem. Phys. Lett.* **2006**, *427*, 201−205.
(30) Laurencin, D.; Gervais, C.; Wong, A.; Coelho, C.; Mauri, F.; Massiot, D.; Smith, M. E.; Bonhomme, C. *J. Am. Chem. Soc.* **2009**, *131*, 13430−13440.
(31) Gervais, C.; Laurencin, D.; Wong, A.; Pourpoint, F.; Labram, J.; Woodward, B.; Howes, A. P.; Pike, K. J.; Dupree, R.; Mauri, F.; Bonhomme, C.; Smith, M. E. *Chem. Phys. Lett.* **2008**, *464*, 42−48.
(32) Laurencin, D.; Wong, A.; Dupree, R.; Smith, M. E. *Magn. Reson. Chem.* **2008**, *46*, 347−350.
(33) Wong, A.; Laurencin, D.; Dupree, R.; Smith, M. E. *Solid State Nucl. Magn. Reson.* **2009**, *35*, 32−36.
(34) Laurencin, D.; Wong, A.; Chrzanowski, W.; Knowles, J. C.; Qiu, D.; Pickup, D. M.; Newport, R. J.; Gan, Z.; Duer, M. J.; Smith, M. E. *Phys. Chem. Chem. Phys.* **2010**, *12*, 1081−1091.
(35) Moudrakovski, I. L.; Alizadeh, R.; Beaudoin, J. J. *Phys. Chem. Chem. Phys.* **2010**, *12*, 6961−6969.
(36) Bonhomme, C.; Gervais, C.; Folliet, N.; Pourpoint, F.; Diogo, C. C.; Lao, J.; Jallot, E.; Lacroix, J.; Nedelec, J.-M.; Iuga, D.; Hanna, J. V.; Smith, M. E.; Xiang, Y.; Du, J.; Laurencin, D. *J. Am. Chem. Soc.* **2012**, *134*, 12611−12628.
(37) Dupree, R.; Howes, A. P.; Kohn, S. C. *Chem. Phys. Lett.* **1997**, *276*, 399−404.
(38) Wong, A.; Laurencin, D.; Wu, G.; Dupree, R.; Smith, M. E. *J. Phys. Chem. A* **2008**, *112*, 9807−9813.

(39) Fox, S.; Büsching, I.; Barklage, W.; Strasdeit, H. *Inorg. Chem.* **2007**, *46*, 818−824.
(40) Kim, E. E.; Sicignano, A.; Eriks, K. *J. Am. Chem. Soc.* **1985**, *107*, 6042−6046.
(41) Schmidbaur, H.; Bach, I.; Wilkinson, D. L.; Müller, G. *Chem. Ber.* **1989**, *122*, 1439−1444.
(42) Wu, G.; Wong, A.; Wang, S. *Can. J. Chem.* **2003**, *81*, 275−283.
(43) Pallister, P. J.; Moudrakovski, I. L.; Ripmeester, J. A. *Phys. Chem. Chem. Phys.* **2009**, *11*, 11487−11500.
(44) Arlin, J.-B.; Florence, A. J.; Johnston, A.; Kennedy, A. R.; Miller, G. J.; Patterson, K. *Cryst. Growth Des.* **2011**, *11*, 1318−1327.
(45) Cole, L. B.; Holt, E. M. *Inorg. Chim. Acta* **1989**, *160*, 195−203.
(46) Barnett, B. L.; Uchtman, V. A. *Inorg. Chem.* **1979**, *18*, 2674−2678.
(47) (a) O'Dell, L. A.; Schurko, R. W. *Chem. Phys. Lett.* **2008**, *464*, 97−102. (b) O'Dell, L. A.; Rossini, A. J.; Schurko, R. W. *Chem. Phys. Lett.* **2009**, *468*, 330−335.
(48) Solomon, I. *Phys. Rev.* **1958**, *110*, 61−65.
(49) Massiot, D.; Farnan, I.; Gautier, N.; Trumeau, D.; Trokiner, A.; Coutures, J. P. *Solid State Nucl. Magn. Reson.* **1995**, *4*, 241−248.
(50) Eichele, K.; Wasylishen, R. E. *WSOLIDS NMR Simulation Software*, Version 1.17.30; Universität Tübingen: Tübingen, Germany, 2001.
(51) Massiot, D.; Fayon, F.; Capron, M.; King, I.; Le Calvé, S.; Alonso, B.; Durand, J.-O.; Bujoli, B.; Gan, Z.; Hoatson, G. *Magn. Reson. Chem.* **2002**, *40*, 70−76.
(52) Segall, M. D.; Lindan, P. J. D.; Probert, M. J.; Pickard, C. J.; Hasnip, P. J.; Clark, S. J.; Payne, M. C. *J. Phys.: Condens. Matter* **2002**, *14*, 2717−2744.
(53) Pickard, C. J.; Mauri, F. *Phys. Rev. B* **2001**, *63*, 245101.
(54) Debuyst, R.; Dejehet, F.; Dekandelaer, M.-C.; Declercq, J.-P.; Germain, G.; van Meerssche, M. *J. Chim. Phys. Phys.-Chim. Biol.* **1979**, *76*, 1117−1124.
(55) Karipides, A.; McKinney, C.; Peiffer, K. *Acta Crystallogr., Sect. C: Cryst. Struct. Commun.* **1988**, *44*, 46−48.
(56) Senkovska, I.; Thewalt, U. *Acta Crystallogr., Sect. C: Cryst. Struct. Commun.* **2005**, *61*, m448−m449.
(57) Wieczorek, M. W.; Błaszczyk, J.; Król, B. W. *Acta Crystallogr., Sect. C* **1996**, *52*, 1193−1198.
(58) Deganello, S.; Kampf, A. R.; Moore, P. B. *Am. Mineral.* **1981**, *66*, 859−865.
(59) Perdew, J. P.; Burke, K.; Ernzerhof, M. *Phys. Rev. Lett.* **1996**, *77*, 3865−3868.
(60) Frisch, M. J.; Trucks, G. W.; Schlegel, H. B.; Scuseria, G. E.; Robb, M. A.; Cheeseman, J. R.; Scalmani, G.; Barone, V.; Mennucci, B.; Petersson, G. A.; Nakatsuji, H.; Caricato, M.; Li, X.; Hratchian, H. P.; Izmaylov, A. F.; Bloino, J.; Zheng, G.; Sonnenberg, J. L.; Hada, M.; Ehara, M.; Toyota, K.; Fukuda, R.; Hasegawa, J.; Ishida, M.; Nakajima, T.; Honda, Y.; Kitao, O.; Nakai, H.; Vreven, T.; Montgomery, J. A., Jr.; Peralta, J. E.; Ogliaro, F.; Bearpark, M.; Heyd, J. J.; Brothers, E.; Kudin, K. N.; Staroverov, V. N.; Kobayashi, R.; Normand, J.; Raghavachari, K.; Rendell, A.; Burant, J. C.; Iyengar, S. S.; Tomasi, J.; Cossi, M.; Rega, N.; Millam, N. J.; Klene, M.; Knox, J. E.; Cross, J. B.; Bakken, V.; Adamo, C.; Jaramillo, J.; Gomperts, R.; Stratmann, R. E.; Yazyev, O.; Austin, A. J.; Cammi, R.; Pomelli, C.; Ochterski, J. W.; Martin, R. L.; Morokuma, K.; Zakrzewski, V. G.; Voth, G. A.; Salvador, P.; Dannenberg, J. J.; Dapprich, S.; Daniels, A. D.; Farkas, Ö.; Foresman, J. B.; Ortiz, J. V.; Cioslowski, J.; Fox, D. J. *Gaussian 09*, Revision A.02; Gaussian, Inc.: Wallingford, CT, 2009.
(61) Adiga, S.; Aebi, D.; Bryce, D. L. *Can. J. Chem.* **2007**, *85*, 496−505.
(62) Widdifield, C. M.; Bryce, D. L. *Can. J. Chem.* **2011**, *89*, 754−763.
(63) Bryce, D. L.; Bultz, E. B.; Aebi, D. *J. Am. Chem. Soc.* **2008**, *130*, 9282−9292.
(64) Deng, Z.-P.; Kang, W.; Zhu, Z.-B.; Huo, L.-H.; Zhao, H.; Gao, S. *Dalton Trans.* **2012**, *41*, 8354−8360.
(65) Plonka, A. M.; Banerjee, D.; Parise, J. B. *Cryst. Growth Des.* **2012**, *12*, 2460−2467.
(66) Huang, Y.-C.; Mou, Y.; Tsai, T. W.-T.; Wu, Y.-J.; Lee, H.-K.; Huang, S.-J.; Chan, J. C. C. *J. Phys. Chem. B* **2012**, *116*, 14295−14301.
(67) Sahoo, B. K. *Phys. Rev. A* **2009**, *80*, 012515.
(68) Burgess, K. M. N.; Xu, Y.; Leclerc, M. C.; Bryce, D. L. *J. Phys. Chem. A* **2013**, *117*, 6561−6570.
(69) Bowers, G. M.; Lipton, A. S.; Mueller, K. T. *Solid State Nucl. Magn. Reson.* **2006**, *29*, 95−103.
(70) Bowers, G. M.; Ravella, R.; Komarneni, S.; Mueller, K. T. *J. Phys. Chem. B* **2006**, *110*, 7159−7164.
(71) Briggman, B.; Oskarson, Å. *Acta Crystallogr., Sect. B: Struct. Sci.* **1977**, *33*, 1900−1906.